Front. Phys. 10, 106801 (2015)
DOI 10.1007/s11467-015-0459-z

REVIEW ARTICLE

Graphene versus MoS_2: A short review

Jin-Wu Jiang

Shanghai Institute of Applied Mathematics and Mechanics, Shanghai Key Laboratory of Mechanics in Energy Engineering, Shanghai University, Shanghai 200072, China

E-mail: jiangjinwu@shu.edu.cn, jwjiang5918@hotmail.com

Received September 16, 2014; accepted November 21, 2014

Graphene and MoS_2 are two well-known quasi two-dimensional materials. This review presents a comparative survey of the complementary lattice dynamical and mechanical properties of graphene and MoS_2, which facilitates the study of graphene/MoS_2 heterostructures. These hybrid heterostructures are expected to mitigate the negative properties of each individual constituent and have attracted intense academic and industrial research interest.

Keywords graphene, molybdenum disulphide, lattice dynamics, mechanical properties

PACS numbers 68.65.-k, 63.22.-m, 62.20.-x

Contents

1 Introduction

Quasi-two-dimensional (Q2D) materials have many novel properties and have attracted intense research interest over the past decades. The Q2D family of materials keeps expanding. The Q2D family currently contains the following materials: graphene, hexagonal boron nitride, two-dimensional (2D) honeycomb silicon, layered transition metal dichalcogenides (including MoS_2 and WS_2), black phosphorus, and 2D ZnO. Among the Q2D family of materials, graphene is the most well known. Novoselov and Geim were awarded the Nobel Prize in physics for graphene in 2010 [1].

The investigations on graphene are extensive but not exhaustive [2]. Nevertheless, these studies provide helpful guidance for understanding the whole Q2D family because many of the experimental set ups (initially for graphene) can be used to perform measurements on other materials in this family. For example, the mechanical properties of single-layer MoS_2 (SLMoS_2) were successfully measured using the same nanoindentation platform as graphene [3, 4]. In the theoretical community, many theorems or approaches, which were initially developed to study graphene, are applicable to other Q2D materials. Some of these extensions may be trivial because of the common two-dimensional nature of these materials. However, the extensions may enable new findings as the Q2D materials have different microscopic structures. For example, the bending modulus of SLMoS_2 can be derived using a similar analytic approach as that used for graphene even though the bending modulus of SLMoS_2 is about seven times larger than that of graphene, owing to its trilayer structure (one Mo layer sandwiched between two S layers) [5–9]. Another example is the puckered micro structure of black phosphorus, which leads to a negative Poisson's ratio in the out-of-plane direction [10].

As a result, graphene has attracted ongoing research interest from both the academic and applied communities. Many review articles have been devoted to graphene [1, 11–19]. In addition, researchers have begun examining possible applications of other Q2D materials, using the knowledge gained from graphene. In particular, MoS_2 has attracted considerable research interest, and many review articles have been published on MoS_2 [20–24].

The present review provides a detailed comparison of the mechanical properties of graphene and SLMoS_2 to clarify the positive and negative properties of the individual materials and to highlight the possible advanced

© The Author(s) 2015. This article is published with open access at www.springer.com/11467

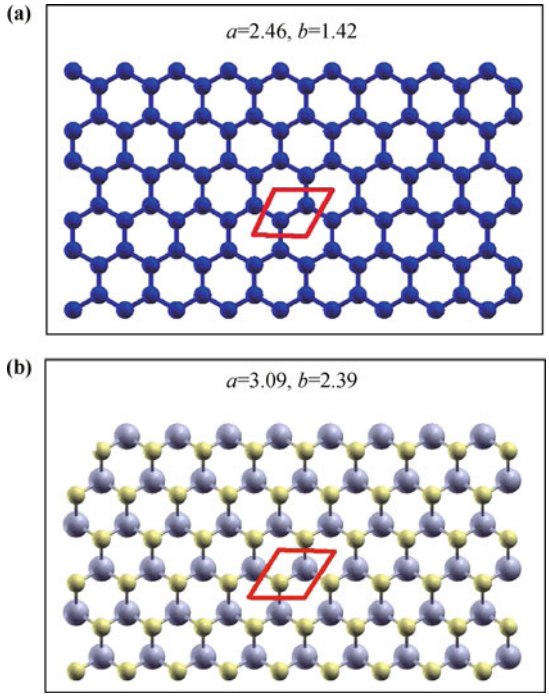

Fig. 1 Top view of the structures of **(a)** graphene and **(b)** $SLMoS_2$. The red rhombus encloses the unit cell in each structure. The numbers are the lattice constant (a) and the bond length (b) in Å.

features and drawbacks of graphene/MoS_2 heterostructures [25]. These hybrid heterostructures are expected to mitigate the negative properties of each individual constituent material. For example, graphene/MoS_2/graphene heterostructures have efficient photon absorption and electron-hole creation properties because of the enhanced light-matter interactions in the $SLMoS_2$ layer [25]. Another experiment recently showed that MoS_2 can be protected from radiation damage with graphene layer coatings [26], exploiting the outstanding mechanical properties of graphene.

In this review, we introduce and compare the following properties for graphene and $SLMoS_2$: the structure, interatomic potential, phonon dispersion, Young's modulus, yield stress, bending modulus, buckling phenomenon, nanomechanical resonator, thermal conductivity, electronic band structure, and optical absorption. We further discuss the properties of the graphene/MoS_2 heterostructure. This article concludes with a table listing the major results for all properties compared in the article.

2 Structure and interatomic potential

Structure. Figure 1(a) shows that graphene has a honeycomb lattice structure with a D_{6h} point group. There are two nonequivalent carbon atoms in the unit cell. These two carbon atoms are reflected onto each other by the inverse symmetry operation from the D_{6h} point group. The lattice constant is $a = 2.46$ Å, and the C-C bond length is $b = a/\sqrt{3} = 1.42$ Å [27].

Figure 1(b) shows the top view of the $SLMoS_2$ structure, which is a trilayer structure with one Mo atomic layer sandwiched between two S atomic layers. The small yellow spheres represent the projection of the two outer S atomic layers onto the Mo atomic layer. The point group for $SLMoS_2$ is D_{3h}. The $\boldsymbol{R}_\pi$ rotation symmetry is broken in $SLMoS_2$. There are two S atoms and one Mo atom in the unit cell. It should be noted that one of the S atoms is not visible due to the trilayer structure. The lattice constant for the in-plane unit cell is $a = 3.09$ Å, and the Mo-S bond length is $b = 2.39$ Å. These values were computed using the Stillinger-Weber (SW) potential [28]; they agree with both the first-principles calculations [29] and the experiments [30].

Interatomic potential. The interactions between the carbon atoms in graphene can be calculated using four different computation cost levels. The first-principles calculation is the most expensive approach for computing the interatomic energy of graphene. Many existing simulation packages can be used for such calculations, including the commercially available Vienna Ab-initio Simulation Package (VASP) [31] and the freely available Spanish Initiative for Electronic Simulations with Thousands of Atoms (SIESTA) package [32]. To reduce the computational cost, Brenner *et al.* developed an empirical potential for carbon-based materials, including graphene [33]. The Brenner potential takes the form of the bond-order Tersoff potential [34] and is able to capture most of the linear properties and many of the nonlinear properties of graphene. For instance, the Brenner potential can describe the formation and breakage of bonds in graphene, providing a good description of its structural, mechanical, and thermal properties. The Tersoff potential [34] or the SW potential [35, 36] provides reasonable predictions for some of the nonlinear and linear properties of graphene. These two empirical potentials have fewer parameters than the Brenner potential, thus they are computationally faster than the Brenner potential. Finally, the linear part of the C-C interactions in graphene can be captured using valence force field models (VFFMs) [37], which have the most inexpensive computational costs.

The potentials of these four computation techniques can also be used for $SLMoS_2$. First-principles calculations can be used for $SLMoS_2$. In 2009, Liang *et al.* parametrized a bond-order potential for $SLMoS_2$ [38], which was based on the bond-order concept underlying the Brenner potential [33]. This Brenner-like potential

was further modified to study the nanoindentations in $SLMoS_2$ thin films using a molecular statics approach [39]. Recently, we parametrized the SW potential for $SLMoS_2$, where the potential parameters were fitted to the phonon spectrum [28]. This potential could easily be used in some of the popular simulation packages, such as the General Utility Lattice Program (GULP) [40] and the Large-Scale Atomic/Molecular Massively Parallel Simulator (LAMMPS) [41]. In 1975, Wakabayashi *et al.* [30]. developed a VFFM to calculate the phonon spectrum in bulk MoS_2. This linear model has been used to study the lattice dynamical properties of some MoS_2-based materials [42–44].

3 Phonon dispersion

A phonon is a quasiparticle in reciprocal space. Each phonon mode describes a particular type of collective vibrations for all of the atoms in the real lattice space. The symmetry of the vibration morphology follows an irreducible representation of the system space group, where the irreducible representations are denoted by the wave vector $\boldsymbol{k}$. The phonon modes are denoted by the wave vector $\boldsymbol{k}$ and the branch index τ, where $\boldsymbol{k}$ is the inter-cell degree of freedom and τ corresponds to the intra-cell degree of freedom. Each phonon mode has a specific angular frequency (ω_k^τ) and eigenvector ($\boldsymbol{\xi}_k^\tau$). For graphene and $SLMoS_2$, each degree of freedom in the real lattice space can be indicated by $(l_1 l_2 s\alpha)$. Here, l_1 and l_2 denote the position of the unit cell, s describes the different atoms in the unit cell, and $\alpha = x, y, z$ is the direction of the axis. The frequency and the eigenvector of the phonon mode can be obtained through diagonalization of the following dynamical matrix:

$$D_{s\alpha;s'\beta}(\boldsymbol{k}) = \frac{1}{\sqrt{m_s m_{s'}}} \sum_{l_1=1}^{N_1} \sum_{l_2=1}^{N_2} K_{00s\alpha;l_1 l_2 s'\beta} \mathrm{e}^{\mathrm{i}\boldsymbol{k}\cdot\boldsymbol{R}_{l_1 l_2}};$$

$$\sum_{s'\beta} D_{s\alpha;s'\beta}(\boldsymbol{k})\, \xi_\beta^{(\tau')}(\boldsymbol{k}|00s') = \omega^{(\tau)2}(\boldsymbol{k}) \xi_\alpha^{(\tau')}(\boldsymbol{k}|00s).$$

The force constant matrix $K_{00s\alpha;l_1 l_2 s'\beta}$ stores the information on the interactions between the two degrees of freedom, $(00s\alpha)$ and $(l_1 l_2 s'\beta)$. The total number of unit cells is given by $N_1 \times N_2$. For the short-range interactions, a summation over (l_1, l_2) can be truncated to the summation over the neighboring atoms.

Figure 2 shows the phonon dispersion of graphene along the high-symmetry ΓKM lines in the first Brillouin zone. The force constant matrix was constructed using the Brenner potential [33]. The inset shows the first Brillouin zone for the hexagonal lattice structure. There are six phonon branches in graphene according to the two nonequivalent carbon atoms in the unit cell. These branches (from low to high frequency) are the z-directional acoustic (ZA), transverse acoustic (TA), longitudinal acoustic (LA), z-directional optical (ZO), transverse optical (TO), and longitudinal optical (LO) branches. The three blue curves in the lower frequency range correspond to the three acoustic branches, while the upper three red curves correspond to the optical branches. The eigenvectors of the six phonon modes at the Γ point in the first Brillouin zone of graphene are displayed in Fig. 3. In the top panel, the three acoustic phonon modes have zero frequency, indicating that the interatomic potential did not vary during rigid translational motion. In the bottom panel, the two in-plane optical phonon modes have almost the same frequency, revealing the isotropic phonon properties for the two in-plane directions in graphene [45].

Figure 4 shows the phonon dispersion of $SLMoS_2$ along the high-symmetry ΓKM lines in the first Brillouin zone. The atomic interactions are described by the SW potential [28]. The inset shows the same first Brillouin zone as that shown for graphene. Each unit cell has one Mo

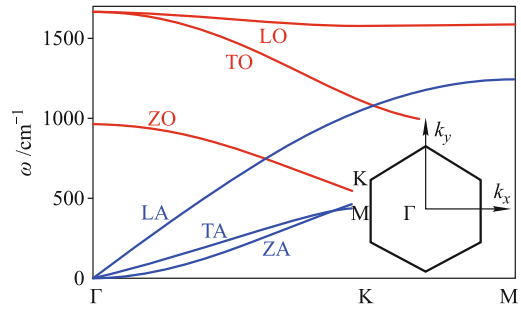

Fig. 2 Phonon dispersion of graphene along the high symmetry ΓKM lines in the Brillouin zone. The interactions between the carbon atoms were determined by the Brenner potential. The inset shows the first Brillouin zone for the hexagonal lattice structure.

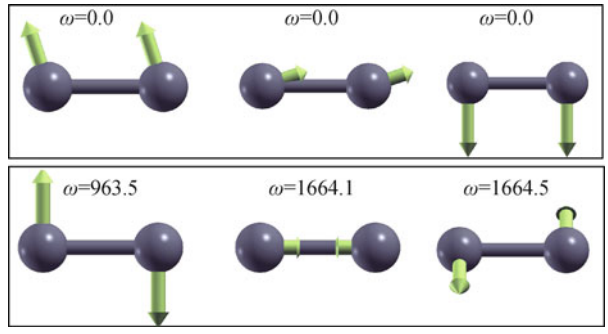

Fig. 3 Eigenvectors for the six phonon modes at the Γ point in the first Brillouin zone of graphene. The arrow attached to each atom represents the vibration component of the atom in the eigenvector. The numbers are the frequencies of each phonon mode with units of cm^{-1}.

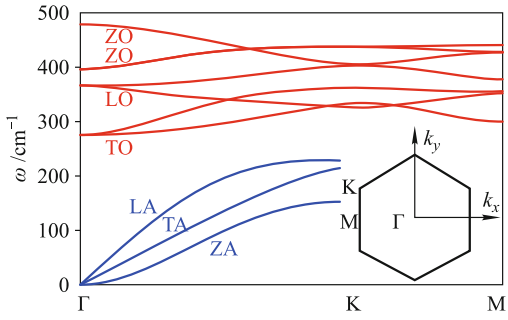

Fig. 4 Phonon dispersion of $SLMoS_2$ along the high symmetry ΓKM lines in the Brillouin zone. The interactions are described by the SW potential. The inset shows the first Brillouin zone for the hexagonal lattice structure.

atom and two S atoms; thus, there are nine branches in the phonon spectrum. The three lower blue curves correspond to the three acoustic branches, while the six upper curves correspond to the optical branches. Figure 5 shows the eigenvectors for the nine phonons at the Γ point in the first Brillouin zone of $SLMoS_2$. There are two interesting shear-like phonon modes and two interlayer breathing-like phonon modes shown in the second row [46]. These interlayer phonon modes are closely related to the interlayer interaction, so they can be used to detect the interlayer coupling in heterostructures.

From the phonon dispersion of graphene and $SLMoS_2$, it is difficult to determine which material has better phonon properties. However, there are two obvious differences in their phonon dispersions. First, the overall spectrum of graphene is higher than that of $SLMoS_2$ by a factor of approximately three. As a result, the phonon modes in graphene can carry more energy than those in $SLMoS_2$ in the thermal transport phenomenon, leading to the stronger thermal transport ability of graphene. Second, there is a distinct energy band gap between the acoustic and optical branches in $SLMoS_2$. This band gap forbids many phonon–phonon scattering channels in $SLMoS_2$; thus, it protects the acoustic phonon modes from being interrupted by the high-frequency optical

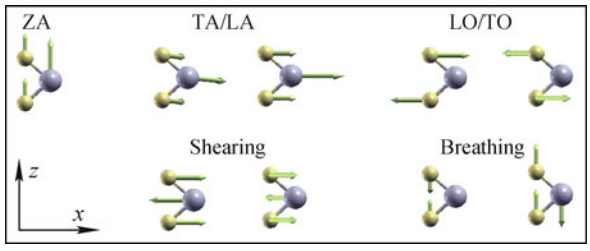

Fig. 5 Eigenvectors for the nine phonon modes at the Γ point in the first Brillouin zone of $SLMoS_2$. There are three acoustic phonon modes, two intra-layer optical modes, two intra-layer shearing modes and two intra-layer breathing modes. The arrows attached to each atom represent the vibration component of the atom in the eigenvector.

phonons [47]. As a result, $SLMoS_2$ nanoresonators have a higher quality (Q)-factor than graphene nanoresonators since the resonant oscillations in $SLMoS_2$ (related to the ZA mode) are affected by weaker thermal vibrations.

4 Mechanical properties

The mechanical properties for both graphene and $SLMoS_2$ have been extensively investigated [48–60]. Here, we discuss several of the basic mechanical properties, including the Young's modulus, yield stress, bending modulus and buckling phenomenon. These mechanical properties are fundamental for the application of graphene or $SLMoS_2$ in nano-devices. Good mechanical stability is essential in nanoscale devices as they are sensitive to external perturbations because of their high surface-to-volume ratio.

Young's modulus. The Young's modulus is given by $Y = E^{2D}/h$, where h is the film thickness and E^{2D} is the thickness-independent effective Young's modulus. We discuss this effective Young's modulus here. The thicknesses were chosen to be 3.35 Å and 6.09 Å for graphene and $SLMoS_2$, respectively. These value are half of the lattice constant in the bulk graphite and MoS_2, respectively. Nanoindentation experiments have measured the effective Young's modulus of graphene to be approximately 335.0 $N{\cdot}m^{-1}$ [3]. This value could be theoretically reproduced using a simple approach in which the nonlinear interactions are estimated from the Tersoff–Brenner potential [61].

For $SLMoS_2$, similar nanoindentation experiments obtained an average value for the effective Young's modulus of 180 ± 60 $N{\cdot}m^{-1}$ in the experiment by Bertolazzi *et al.* [62], and 120 ± 30 $N{\cdot}m^{-1}$, measured by Cooper *et al.* [4, 63] Recently, Liu *et al.* performed similar nanoindentation experiments on chemical-vapor-deposited $SLMoS_2$, obtaining an effective Young's modulus of about 170 $N{\cdot}m^{-1}$ [64]. The nanoindentation set up has also been used to study the Young's modulus of thicker MoS_2 films [65]. The theoretical prediction of the effective Young's modulus is 139.5 $N{\cdot}m^{-1}$ for $SLMoS_2$, based on the SW potential [28].

Yield stress. The nanoindentation measurements can also be used to determine the yield stress ($\sigma_{\rm int}$, the maximum of the stress-strain curve). Lee *et al.* determined the yield stress to be 42 ± 4 $N{\cdot}m^{-1}$ for graphene [3]. Moreover, the yield stresses obtained with the continuum elasticity theory were 42.4 $N{\cdot}m^{-1}$ using a tight-binding atomistic model [66] and 44.4 $N{\cdot}m^{-1}$ using the Brenner potential [67]. While the elasticity continuum simulation provided an isotropic value for the yield stress in

graphene, microscopic atomic models have predicted the yield stress to be dependent on the chirality in graphene. First-principles calculations predicted the yield stress to be 40.5 N·m^{-1} in the zigzag direction and 36.9 N·m^{-1} in the armchair direction in graphene [68]. Molecular mechanics simulations obtained a yield stress of 36.9 N·m^{-1} in the zigzag direction and 30.2 N·m^{-1} in the armchair direction in graphene [68]. Both of the atomic models showed that graphene has a higher yield stress in the zigzag direction than in the armchair direction. Note that the definition of the armchair and zigzag directions in Ref. [48] opposes that in Ref. [68]. We have retained the definition from Ref. [68], where the armchair direction is along the direction of the carbon–carbon bonds.

In $SLMoS_2$, nanoindentation experiments found that the yield stress was 15 ± 3 N·m^{-1}, determined by Bertolazzi *et al.* [62], and 16.5± N·m^{-1}, determined by Cooper *et al.* [4, 63] In the first-principles calculations, the yield stress was predicted to be 17.5 N·m^{-1} under a biaxial strain in $SLMoS_2$ [69]. While the studies on the yield stress in $SLMoS_2$ are limited, the novel structure transition in $SLMoS_2$ has received considerable attention [70–73]. In this structure transition, the outer two S atomic layers are shifted relative to each other, leading to abrupt changes in the electronic and phonon properties in $SLMoS_2$. This structure transition is the result of the trilayer configuration of $SLMoS_2$ and is not observed in graphene.

Bending modulus. Graphene is extremely soft in the out-of-plane direction owing to its one-atom-thick structure [74–78]. Graphene is so thin that it has an extremely small bending modulus, which can be explained by the well-known relationship in the shell theorem, $D = E^{2D}h^2/(12(1-\nu^2))$, where h is the thickness and ν is Poisson's ratio. The bending modulus of graphene has been derived analytically from two equivalent approaches; the obtained value was 1.17 eV using the geometric approach with interactions described by the VFFM [5, 6] and 1.4 eV from the exponential Cauchy-Born rule using the Brenner potential [7, 8]. Note that these two approaches are equivalent to each other, and the difference in the bending modulus is primarily a result of the different potentials used in these two studies.

A similar analytic approach was used to derive the bending modulus of $SLMoS_2$ using the SW potential [9]. The bending modulus of $SLMoS_2$ is 9.61 eV, which is larger than that of graphene by a factor of seven. The large bending modulus of $SLMoS_2$ is due to its trilayer atomic structure, which results in more interaction terms inhibiting the bending motion. The bending modulus can be calculated as follows:

$$D = \frac{\partial^2 W}{\partial \kappa^2}, \tag{1}$$

where W is the bending energy density and κ is the bending curvature. For $SLMoS_2$, the bending energy can be written as [9]

$$D = \sum_q \frac{\partial^2 W}{\partial r_q^2}\left(\frac{\partial r_q}{\partial \kappa}\right)^2 + \sum_q \frac{\partial^2 W}{\partial \theta_q^2}\left(\frac{\partial \theta_q}{\partial \kappa}\right)^2, \tag{2}$$

where r_q and θ_q are the geometrical parameters in the empirical potential expressions. This formula is substantially different from the bending modulus formula for graphene [79]. Specifically, the first derivatives, $\frac{\partial r_q}{\partial \kappa}$ and $\frac{\partial \theta_q}{\partial \kappa}$, are nonzero owing to the trilayer structure of $SLMoS_2$. As a result, the bending motion in $SLMoS_2$ will be counteracted by an increasing number of cross-plane interactions.

Buckling phenomenon. The buckling phenomenon can be disastrous in nanoscale devices; however, it can be useful in some situations [80–83]. The Euler buckling theorem states that the buckling critical strain can be determined from the effective Young's modulus and the bending modulus through the following formula [84]:

$$\epsilon_c = -\frac{4\pi^2 D}{E^{2D}L^2}, \tag{3}$$

where L is the length of the system. For graphene, the values of $E^{2D} = 335$ N·m^{-1} and $D = 1.4$ eV, described above, give the following explicit value for the buckling critical strain:

$$\epsilon_c = -\frac{2.64}{L^2}. \tag{4}$$

The length (L) is given in Angstroms (Å).

For $SLMoS_2$, the values of $E^{2D} = 139.5$ N·m^{-1} and $D = 9.61$ eV, described above, can be used to obtain the following explicit formula for the buckling critical strain:

$$\epsilon_c = -\frac{43.52}{L^2}. \tag{5}$$

For samples of the same length, the buckling critical strain for $SLMoS_2$ is twenty times larger than of graphene; in other words, $SLMoS_2$ does not easily buckle under external compression. This phenomenon has been examined with both molecular dynamics (MD) simulations and phonon analysis [71, 85].

In our discussion of the mechanical properties of graphene and $SLMoS_2$, we have shown that graphene has a larger Young's modulus, larger yield stress, and is more flexibility than $SLMoS_2$. On the other hand, $SLMoS_2$ has a higher bending modulus and does not buckle as readily as graphene under external compression. Hence, in terms of the mechanical properties, it is more advan-

tageous for graphene and $SLMoS_2$ to be used together in a heterostructure to mitigate the negative mechanical properties of each constituent.

5 Nanomechanical resonators

Nanoresonators based on two-dimensional materials such as graphene and $SLMoS_2$ are promising candidates for ultra-sensitive mass sensing and detection because of their large surface areas and small masses [86–94]. For sensing applications, it is important that the nanoresonator exhibits a high Q-factor because the sensitivity of a nanoresonator is inversely proportional to its Q-factor [95]. The Q-factor is a quantity that records the total number of oscillation cycles of the resonator before its resonant oscillation decays considerably. Hence, a weaker energy dissipation leads to a higher Q-factor.

For graphene nanoresonators, the Q-factor increases exponentially with decreasing temperatures [96, 97], $T^{-\alpha}$. Zande *et al.* [96] found that the exponent α=0.35± 0.05 for temperatures below 40 K. For temperatures above 40 K, $\alpha = 2.3 \pm 0.1$. Chen *et al.* [97] observed a similar transition in the Q-factor. This continuous transition for the temperature dependence of the Q-factor is attributed to the diffusion of adsorbs in the out-of-plane direction on the surface of the graphene layer [98, 99]. The MD simulations also predicted a discontinuous transition in the Q-factor at the low temperature of 7.0 K, which is caused by the in-plane diffusion of adsorbs on the graphene surface [98]. A very high Q-factor has been achieved in the laboratory at low temperatures. Bunch *et al.* observed a Q-factor of 9000 for a graphene nanoresonator at 10 K [96]. Chen *et al.* also found that the Q-factor increased with decreasing temperature, reaching 10^4 at 5 K [97]. Eichler *et al.* [100] found that the Q-factor of a graphene nanoresonator reached 10^5 at 90 mK.

For $SLMoS_2$, two recent experiments demonstrated the nanomechanical resonant behavior in $SLMoS_2$ [101] and few-layer MoS_2 [102]. Castellanos-Gomez *et al.* found that the figure of merit, i.e., the frequency-Q-factor product, is $f_0 \times Q \approx 2 \times 10^9$ Hz for $SLMoS_2$ [101]. Lee *et al.* found that few-layer MoS_2 resonators exhibit a high figure of merit of $f_0 \times Q \approx 2 \times 10^{10}$ Hz [102]. The high Q-factor of $SLMoS_2$ could be attributed to the energy band gap in the phonon dispersion of $SLMoS_2$, which protects the resonant oscillations from being scattered by thermal vibrations [47]. As a result, the Q-factor of $SLMoS_2$ nanoresonators was predicted to be higher than that of graphene nanoresonators by at least a factor of four.

Although it has been theoretically predicted that MoS_2 will have better mechanical resonance behavior than graphene, experiments on MoS_2 nanoresonators are limited. More measurements are needed to examine the nanoresonator properties, such as the mass sensitivity. Furthermore, the sensor application of the nanoresonators depends on the level of low frequency $1/f$ noise, which is a limiting factor for communication applications and sensor sensitivity as well as the selectivity of graphene and MoS_2 nanoresonators [103–109].

6 Thermal conductivity

The thermal transport phenomenon occurs when there is a temperature gradient in a material, and thermal energy can be carried by phonons or electrons. Moreover, the electronic thermal conductivity is important for metals. For graphene, phonons are the primary contributors to the thermal conductivity, and electronic thermal conductivity is less than 1% of the overall thermal conductivity [110, 111]. Thus, only the phonon (lattice) thermal conductivity will be discussed for the graphene. The thermal transport is in the ballistic regime at low temperatures with weak phonon–phonon scattering [112, 113]. For ballistic transport, the thermal conductivity (κ) is proportional to the length (L) of the system: $\kappa \propto L$. At high temperatures, the phonon-phonon scattering is strong, so the thermal transport is in the diffusive regime. For diffusive transport, the thermal conductivity is related to the thermal current density (J) and the temperature gradient (∇T) through the Fourier law: $\kappa = -\nabla T/J$.

In bulk materials, the room temperature thermal conductivity is normally a size-independent constant. Graphene has high thermal conductivity [49, 114–124], which behaves irregularity with the length in Q2D graphene; in other words, the in-plane thermal conductivity is not constant and increases with increasing sample length [125–133]. For 10 nm long graphene, the room-temperature thermal conductivity from the MD simulation is on the order of 60 $W{\cdot}m^{-1}{\cdot}K^{-1}$ [134]. The thermal conductivity increased quickly with increasing length, reaching 250 $W{\cdot}m^{-1}{\cdot}K^{-1}$ for 300 nm long graphene [129]. For a length of 4.0 μm, graphene had a thermal conductivity near [135] 2500 $W{\cdot}m^{-1}{\cdot}K^{-1}$. For graphene samples larger than 10 μm, the thermal conductivity varies in the range from 1500 $W{\cdot}m^{-1}{\cdot}K^{-1}$ to 5000 $W{\cdot}m^{-1}{\cdot}K^{-1}$, depending on the sample size and quality [129, 136, 137]. Balandin *et al.* reported the highest value of 5000 $W{\cdot}m^{-1}{\cdot}K^{-1}$ for a 20 μm sample. Thus, these studies show that the thermal conductivity in graphene increases with increasing dimension, even though the sample size

is larger than the phonon mean free path [137]. However, there is no universally accepted underlying mechanism for the size dependence of the thermal conductivity in graphene [127, 132, 138–141]. In the out-of-plane direction, the thermal conductivity for graphene decreases with increasing layer number as there are more phonon-phonon scattering channels in thicker few-layer graphene [138, 142–149].

For MoS_2, a recent experiment by Sahoo *et al.* found that few-layer MoS_2 has a thermal conductivity near [150] 52 $W{\cdot}m^{-1}{\cdot}K^{-1}$, which is much lower than that in thick graphene layers (1000 $W{\cdot}m^{-1}{\cdot}K^{-1}$) [142]. Although there are currently no measurements on the thermal conductivity of $SLMoS_2$, this topic has attracted increasing interest in the theoretical community [151–153]. In 2010, Varshney *et al.* performed force-field-based MD simulations to study the thermal transport in $SLMoS_2$ [151]. In 2013, two first-principles calculations were performed to investigate the thermal transport in $SLMoS_2$ in the ballistic transport regime [152, 153]. The predicted room-temperature thermal conductivity in the ballistic regime was below 800 $W{\cdot}m^{-1}{\cdot}K^{-1}$ for a 1.0 μm long $SLMoS_2$ sample [153]. This value is considerably lower than the ballistic thermal conductivity of 5000 $W{\cdot}m^{-1}{\cdot}K^{-1}$ for a graphene sample with the same length [154]. The smaller thermal conductivity of $SLMoS_2$ in the ballistic regime was caused by the lower phonon spectrum in $SLMoS_2$, which is lower than that of graphene by a factor of three. Thus, each phonon mode in $SLMoS_2$ carries less thermal energy than that in graphene. In 2013, we performed MD simulations to predict the room-temperature thermal conductivity of $SLMoS_2$, which was 6.0 $W{\cdot}m^{-1}{\cdot}K^{-1}$ for a 4.0 nm long system [28]. More recently, the size dependence of the thermal conductivity in $SLMoS_2$ was studied with MD simulations. The value obtained was below 2.0 $W{\cdot}m^{-1}{\cdot}K^{-1}$ for a system with a length shorter than 120.0 nm [155].

As we have shown, graphene has a much higher thermal conductivity than $SLMoS_2$. The high thermal conductivity of graphene is useful for transporting heat out of electronic transistor devices; thus, graphene can be used to enhance the thermal transport capability of some composites [156–164]. Current transistors operate at very high speeds and are damaged by the inevitable Joule heating if the generated heat energy is not pumped out effectively. In this sense, graphene has better thermal conductivity properties than $SLMoS_2$.

7 Electronic band structure

The electronic band structure is fundamental for electronic processes such as transistor performance. In particular, the value of the electronic band gap determines whether the material is a conductor (zero band gap), semiconductor (moderate band gap), or insulator (large band gap).

Electrons in graphene behavior like Dirac fermions; i.e., the electronic energy dispersion is linear near the Brillouin zone corner. The velocity of this Dirac fermion is at 1/300 the speed of light [165–167]. The Dirac fermion was found to be closely related to the mirror plane symmetry in AB-stacked few-layer graphene; i.e., Dirac fermions exist in AB-stacked few-layer graphene with an odd number of layers, and the electronic spectrum becomes parabolic in AB-stacked few-layer graphene with an even number of layers [168]. Interestingly, Dirac fermions are also present in twisted bilayer graphene [169] due to the effective decoupling of the two graphene layers by the twisting defect; that is, the mirror plane symmetry is effectively recovered in twisted bilayer graphene. The Dirac cone at the Brillouin zone corner has a zero band gap in graphene, which is mainly contributed by free π electrons [170]. For electronic devices, like transistors, a finite band gap is desirable, and various techniques have been invented to open an electronic band gap in graphene. Strain engineering can be used to generate a finite band gap of 0.1 eV with a 24% uniaxial strain [171]. Guinea *et al.* applied triangular symmetric strains to generate a band gap over 0.1 eV, which is observable at room temperature [172]. A finite band gap can also be opened by confining the graphene structure in a nanoribbon form, where the band gap increases with decreasing ribbon width [173].

Electrons in $SLMoS_2$ are normal fermions with parabolic energy dispersion, and $SLMoS_2$ is a semiconductor with a direct band gap above 1.8 eV [174–177]. This finite band gap endorses $SLMoS_2$ for transistor applications [178, 179]. Similar to graphene, the band gap in $SLMoS_2$ can also be modulated by strain engineering. First-principles calculations predict a semiconductor-to-metal transition in $SLMoS_2$ using biaxial compression or tension [180]. An experiment by Eknapakul *et al.* shows that a uniaxial tensile mechanical strain of 1.5% can produce a direct-to-indirect band gap transition [181]. With an increasing number of layers, the electronic band gap for few-layer MoS_2 undergoes a direct-to-indirect transition, decreasing to a value of 1.2 eV for bulk MoS_2 [182].

From these comparisons, we find that $SLMoS_2$ possesses a finite band gap prior to any gap-opening engineering. Consequently, $SLMoS_2$ may be more competitive than graphene for applications in transistors, optoelectronics, energy harvesting, and other nano-material fields.

8 Optical absorption

The optical properties of Q2D materials are important for their applications in photodetectors, phototransitors, or other photonic nanodevices. Moreover, the photocarriers in these Q2D materials may have significantly different behavior from conventional semiconductors due to their particular configurations.

Graphene has a Dirac cone electron band structure with zero band gap [166, 167]. Related to this unique band structure, graphene can absorb about 2% of the incident light over a broad wavelength, which is strong considering its single-layer structure [183]. Xia *et al.* demonstrated an ultra-fast photodetector behavior for graphene, where the photoresponse did not degrade for optical intensity modulations up to 40 GHz and where the intrinsic band width was estimated to be above 500 GHz [184]. However, the photoresponsivity for graphene is low due to its zero bandgap.

On the other hand, $SLMoS_2$ has a direct band gap of about 1.8 eV [174, 175]. This optical-range band gap leads to a high absorption coefficient for incident light, so $SLMoS_2$ has very high sensitivity in photon detection [182]. Lopez-Sanchez *et al.* found that the photoresponsivity of $SLMoS_2$ can be as high as 880 $A{\cdot}W^{-1}$ for incident light at the wavelength of 561 nm, and the photoresponse is in the 400–680 nm range [185]. This high photoresponsivity together with fast light emission enables $SLMoS_2$ to be used as ultra sensitive phototransistors with good device mobility and large ON current. In phototransistors, the electron-hole pair can be efficiently generated by photoexcitions in doped $SLMoS_2$, which join the doping-induced charges to form bound states of two electrons and one hole. As a result, the carrier effective mass is considerably increased, and the photoconductivity can be decreased [186].

Regarding the optical properties of graphene and $SLMoS_2$, graphene shows very fast photo detection, while $SLMoS_2$ has very sensitive photo detection. Considering these complementary property, heterostructures designed with these two materials may be fruitful.

9 Graphene/MoS_2 heterostructure

Thus far, we have compared several of the properties of graphene and $SLMoS_2$. This section is devoted to studies on the close relationship between these two materials. As graphene and $SLMoS_2$ have complementary physical properties, it is natural to combine graphene and $SLMoS_2$ in specific ways to create heterostructures that mitigate any negative properties [25, 26, 187–197].

A few experiments have investigated the advanced properties of graphene/MoS_2 heterostructures. Britnell *et al.* found that graphene/MoS_2 heterostructures have high quality photon absorption and electron-hole creation properties because of the enhanced light-matter interactions in the $SLMoS_2$ layer [25]. As discussed earlier, graphene has outstanding mechanical properties. These mechanical properties have been used to protect MoS_2 films from radiation damage [26]. Recently, Larentis *et al.* measured the electron transport in graphene/MoS_2 heterostructures and observed a negative compressibility in the MoS_2 component [191]. This surprising phenomenon could be explained based on the interplay between the Dirac and parabolic bands for graphene and MoS_2, respectively. Yu *et al.* fabricated high-performance electronic circuits based on a graphene/MoS_2 heterostructure with MoS_2 as the transistor channel and graphene as the contact electrodes and the circuit interconnects [198].

Although experimentalists have shown great interest in graphene/MoS_2 heterostructures, the corresponding theoretical efforts have been limited until recently. Two first-principle studies have predicted the inter-layer space and binding energy for the heterostructure at –21.0 meV and 3.66 Å, respectively [199], and at –23.0 meV and 3.32 Å, respectively [197]. Using these two quantities [200], a set of Lennard-Jones potential parameters were determined as $\epsilon = 3.95$ meV and $\sigma = 3.625$ Å, with a cutoff of 10.0 Å. These potential parameters were used to study the tension-induced structure transition of the graphene/MoS_2/graphene heterostructure. Moreover, the Young's modulus of the graphene/MoS_2/graphene heterostructure could be predicted by the following rule of mixtures, based on the arithmetic average [201]:

$$Y_{GMG} = Y_G f_G + Y_M f_M, \tag{6}$$

where Y_{GMG}, Y_G and Y_M are the Young's moduli of the heterostructure, graphene, and $SLMoS_2$, respectively. Furthermore, $f_G = 2V_G/(2V_G + V_M) = 0.524$ is the volume fraction for the two outer graphene layers in the heterostructure, and $f_M = V_M/(2V_G + V_M) = 0.476$ is the volume fraction for the inner $SLMoS_2$ layer. The thicknesses were 3.35 Å and 6.09 Å for single-layer graphene and $SLMoS_2$, respectively. At room temperature, Young's modulus was 859.69 GPa for graphene and 128.75 GPa for $SLMoS_2$. From this mixing rule, the upper-bound of the Young's modulus for the heterostructure was 511.76 GPa.

The total strain of the graphene/MoS_2/graphene heterostructure was about 0.26, which is much smaller than

Table 1 The properties of graphene and $SLMoS_2$ discussed in this review.

Properties	Graphene	$SLMoS_2$
Structure	D_{6h}; $a = 2.46$ Å; $b = 1.42$ Å (Ref. [27])	D_{3h}; $a = 3.09$ Å; $b = 2.39$ Å (Ref. [28])
Interaction	*ab initio*; Brenner; SW; VFFM	*ab initio*; Brenner; SW; VFFM
Phonon dispersion	$\omega_{\rm op} \approx 1664.5$ cm^{-1}; $\omega_{\rm gap} = 0$	$\omega_{\rm op} \approx 478.8$ cm^{-1}; $\omega_{\rm gap} = 25.0$ cm^{-1}
Young's modulus	$E^{2D} = 335.0$ N·m^{-1} (Ref. [3])	$E^{2D} = 180 \pm 60$ N·m^{-1} (Ref. [62]) $E^{2D} = 120 \pm 30$ N·m^{-1} (Ref. [4]) $E^{2D} = 170$ N·m^{-1} (Ref. [64]) $E^{2D} = 139.5$ N·m^{-1} (Ref. [28])
Yield stress	$\sigma_{\rm int} = 42 \pm 4$ N·m^{-1} (Ref. [3]) $\sigma_{\rm int} = 42.4$ N·m^{-1} (Ref. [66]) $\sigma_{\rm int} = 44.4$ N·m^{-1} (Ref. [67]) $\sigma_{\rm int}^{\rm zig} = 40.5$ N·m^{-1}, $\sigma_{\rm int}^{\rm arm} = 36.9$ N·m^{-1} (Ref. [48]) $\sigma_{\rm int}^{\rm zig} = 36.9$ N·m^{-1}, $\sigma_{\rm int}^{\rm arm} = 30.2$ N·m^{-1} (Ref. [68])	$\sigma_{\rm int} = 15 \pm 3$ N·m^{-1} (Ref. [62]) $\sigma_{\rm int} = 16.5$ N·m^{-1} (Refs. [4, 63]) $\sigma_{\rm int} = 17.5$ N·m^{-1} (Ref. [69])
Bending modulus	$D = 1.17$ eV (Refs. [5, 6]), 1.4 eV (Refs. [7, 8])	$D = 9.61$ eV (Ref. [9])
Buckling strain	$\epsilon_c = -\frac{2.64}{L^2}$	$\epsilon_c = -\frac{43.52}{L^2}$
Nanoresonator	$f_0 \times Q = 6.3 \times 10^{11}$ Hz (10 K, Ref. [96]) $f_0 \times Q = 1.82 \times 10^{12}$ Hz (5 K, Ref. [97]) $f_0 \times Q = 1.56 \times 10^{13}$ Hz (90 mK, Ref. [100])	$f_0 \times Q \approx 2 \times 10^9$ Hz (300 K, Ref. [101])
	$f_0 \times Q = 6.4T^{-1.2} \times 10^3$ THz (Ref. [47])	$f_0 \times Q = 2.4T^{-1.3} \times 10^4$ THz (Ref. [47])
Thermal conductivity	5000 W·m^{-1}·K^{-1} (ballistic, $L = 1$ μm, Ref. [154])	800 W·m^{-1}·K^{-1} (ballistic, $L = 1$ μm, Refs. [152, 153])
	60 W·m^{-1}·K^{-1} ($L = 10$ nm, Ref. [134]) 250 W·m^{-1}·K^{-1} ($L = 300$ nm, Ref. [129]) $\kappa > 1500$ W·m^{-1}·K^{-1} ($L > 4$ μm, Refs. [129, 135–137])	6 W·m^{-1}·K^{-1} ($L = 4$ nm, Ref. [28]) 2 W·m^{-1}·K^{-1} ($L = 120$ nm, Ref. [155])
	1000 W·m^{-1}·K^{-1} (thick graphene layers, Ref. [142])	52 W·m^{-1}·K^{-1} (thick MoS_2 layers, Ref. [150])
Electronic band	Dirac cone; $E_{\rm gap} = 0$ (Refs. [166, 167])	parabolic; $E_{\rm gap} \approx 1.8$ eV (direct, Refs. [174, 175])
Optical absorption	fast photoresponse (Ref. [184]) large band width (Ref. [184]) low photoresponsivity (0.5 mA·W^{-1}, Ref. [184])	high photoresponsivity (880 A·W^{-1}, Ref. 185)

the value of 0.40 for $SLMoS_2$ [200]. Under large mechanical tension, the heterostructure collapsed from the buckling of the outer graphene layers. When the heterostructure was stretched in the longitudinal direction, these graphene layers were compressed in the lateral direction by Poisson-induced stress.

10 Conclusions

We have compared the mechanical properties of graphene and $SLMoS_2$. The primary results of this comparison are tabulated in Table 1. Moreover, Table 1 serves as a resource for predicting the corresponding properties of graphene/MoS_2 heterostructures.

Acknowledgements This work was supported by the Recruitment Program of Global Youth Experts of China and start-up funding from Shanghai University.

Open Access This article is distributed under the terms of the Creative Commons Attribution License which permits any use, distribution, and reproduction in any medium, provided the original author(s) and the source are credited.

References and notes

1. A. K. Geim and K. S. Novoselov, The rise of graphene, *Nat. Mater.* 6(3), 183 (2007)
2. A. H. C. Neto and K. Novoselov, New directions in science and technology: Two-dimensional crystals, *Rep. Prog. Phys.* 74(8), 082501 (2011)
3. C. Lee, X. Wei, J. W. Kysar, and J. Hone, Measurement of the elastic properties and intrinsic strength of mono-layer graphene, *Science* 321(5887), 385 (2008)
4. R. C. Cooper, C. Lee, C. A. Marianetti, X. Wei, J. Hone, and J. W. Kysar, Nonlinear elastic behavior of two-dimensional molybdenum disulfide, *Phys. Rev. B* 87(3), 035423 (2013)
5. Z. C. Ouyang, Z. B. Su, and C. L. Wang, Coil formation in multishell carbon nanotubes: Competition between curvature elasticity and interlayer adhesion, *Phys. Rev. Lett.* 78(21), 4055 (1997)
6. Z. C. Tu and Z. C. Ou-Yang, Single-walled and multiwalled carbon nanotubes viewed as elastic tubes with the effective Young's moduli dependent on layer number, *Phys. Rev. B* 65(23), 233407 (2002)
7. M. Arroyo and T. Belytschko, An atomistic-based nite defor-

mation membrane for single layer crystalline films, *J. Mech. Phys. Solids* 50(9), 1941 (2002)

8. Q. Lu, M. Arroyo, and R. Huang, Elastic bending modulus of monolayer graphene, *J. Phys. D: Appl. Phys.* 42(10), 102002 (2009)
9. J. W. Jiang, Z. Qi, H. S. Park, and T. Rabczuk, Elastic bending modulus of single-layer molybdenum disul-phide (MoS_2): Finite thickness effect, *Nanotechnology* 24(43), 435705 (2013)
10. J. W. Jiang and H. S. Park, Negative Poisson's ratio in single-layer black phosphorus, *Nat. Commun.* 5, 4727 (2014)
11. A. C. Ferrari, Raman spectroscopy of graphene and graphite: Disorder, electron-phonon coupling, doping and nonadiabatic effects, *Solid State Commun.* 143(1–2), 47 (2007)
12. A. H. Castro Neto, N. M. R. Peres, K. S. Novoselov, and A. K. Geim, The electronic properties of graphene, *Rev. Mod. Phys.* 81(1), 109 (2009)
13. A. K. Geim, Graphene: Status and prospects, *Science* 324(5934), 1530 (2009)
14. L. M. Malard, M. A. Pimenta, G. Dresselhaus, and M. S. Dressel-haus, Raman spectroscopy in graphene, *Physics Reports* 473, 51 (2009)
15. C. N. R. Rao, A. K. Sood, K. S. Subrahmanyam, and A. Govin-daraj, Graphene: The new two-dimensional nanomaterial, *Angew. Chem. Int. Ed.* 48(42), 7752 (2009)
16. M. J. Allen, V. C. Tung, and R. B. Kaner, Honeycomb carbon: A review of graphene, *Chem. Rev.* 110(1), 132 (2010)
17. F. Bonaccorso, Z. Sun, T. Hasan, and A. C. Ferrari, Graphene photonics and optoelectronics, *Nat. Photonics* 4(9), 611 (2010)
18. F. Schwierz, Graphene transistors, *Nat. Nanotechnol.* 5(7), 487 (2010)
19. A. A. Balandin, Thermal properties of graphene and nanostructured carbon materials, *Nat. Mater.* 10(8), 569 (2011)
20. Q. H. Wang, K. Kalantar-Zadeh, A. Kis, J. N. Coleman, and M. S. Strano, Electronics and optoelectronics of two-dimensional transition metal dichalcogenides, *Nat. Nanotechnol.* 7(11), 699 (2012)
21. M. Chhowalla, H. S. Shin, G. Eda, L. Li, K. P. Loh, and H. Zhang, The chemistry of two-dimensional layered transition metal dichalcogenide nanosheets, *Nat. Chem.* 5(4), 263 (2013)
22. M. Xu, T. Liang, M. Shi, and H. Chen, Graphene-like two-dimensional materials, *Chem. Rev.* 113(5), 3766 (2013)
23. S. Z. Butler, S. M. Hollen, L. Cao, Y. Cui, J. A. Gupta, H. R. Gutiérrez, T. F. Heinz, S. S. Hong, J. Huang, A. F. Ismach, E. Johnston-Halperin, M. Kuno, V. V. Plashnitsa, R. D. Robinson, R. S. Ruoff, S. Salahuddin, J. Shan, L. Shi, M. G. Spencer, M. Terrones, W. Windl, and J. E. Goldberger, Progress, challenges, and opportunities in two-dimensional materials beyond graphene, *ACS Nano* 7(4), 2898 (2013)
24. X. Huang, Z. Zeng, and H. Zhang, Metal dichalcogenide nanosheets: Preparation, properties and applications, *Chem. Soc. Rev.* 42(5), 1934 (2013)
25. L. Britnell, R. M. Ribeiro, A. Eckmann, R. Jalil, B. D. Belle, A. Mishchenko, Y.J. Kim, R. V. Gorbachev, T. Georgiou, S. V. Morozov, A. N. Grigorenko, A. K. Geim, C. Casiraghi, A. H. C. Neto, and K. S. Novoselov, Strong light-matter interactions in heterostructures of atomically thin films, *Science* 340(6138), 1311 (2013)
26. R. Zan, Q. M. Ramasse, R. Jalil, T. Georgiou, U. Bangert, and K. S. Novoselov, Control of radiation damage in MoS_2 by graphene encapsulation, *ACS Nano* 7(11), 10167 (2013)
27. R. Saito, G. Dresselhaus, and M. S. Dresselhaus, Physical Properties of Carbon Nanotubes, London: Imperial College, 1998
28. J. W. Jiang, H. S. Park, and T. Rabczuk, Molecular dynamics simulations of single-layer molybdenum disulphide (MoS_2): Stillinger–Weber parametrization, mechanical properties, and thermal conductivity, *J. Appl. Phys.* 114(6), 064307 (2013)
29. A. Molina-Sánchez and L. Wirtz, Phonons in single-layer and few-layer MoS_2 and WS_2, *Phys. Rev. B* 84(15), 155413 (2011)
30. N. Wakabayashi, H. G. Smith, and R. M. Nicklow, Lattice dynamics of hexagonal MoS_2 studied by neutron scattering, *Phys. Rev. B* 12(2), 659 (1975)
31. G. Kresse and J. Furthmuller, Efficient iterative schemes for ab initio total-energy calculations using a plane-wave basis set, *Phys. Rev. B* 54(16), 11169 (1996)
32. J. M. Soler, E. Artacho, J. D. Gale, A. Garcia, J. Jun-quera, P. Ordejon, and D. Sánchez-Portal, The siesta method for ab initio ordern materials simulation, *J. Phys.: Condens. Matter* 14(11), 2745 (2002) (Code available from http://www.icmab.es/dmmis/leem/siesta/.)
33. D. W. Brenner, O. A. Shenderova, J. A. Harrison, S. J. Stuart, B. Ni, and S. B. Sinnott, A second-generation reactive empirical bond order (REBO) potential energy expression for hydrocarbons, *J. Phys.: Condens. Matter* 14(4), 783 (2002)
34. J. Tersoff, Empirical interatomic potential for carbon, with applications to amorphous carbon, *Phys. Rev. Lett.* 61(25), 2879 (1988)
35. F. H. Stillinger and T. A. Weber, Computer simulation of local order in condensed phases of silicon, *Phys. Rev. B* 31(8), 5262 (1985)
36. F. F. Abraham and I. P. Batra, Theoretical interpretation of atomic force microscope images of graphite, *Surf. Sci.* 209(1–2), L125 (1989)
37. T. Aizawa, R. Souda, S. Otani, Y. Ishizawa, and C. Oshima, Bond softening in monolayer graphite formed on transition-metal carbide surfaces, *Phys. Rev. B* 42(18), 11469 (1990)
38. T. Liang, S. R. Phillpot, and S. B. Sinnott, Parametrization of a reactive many-body potential for Mo-S systems, *Phys. Rev. B* 79(24), 245110 (2009)
39. J. A. Stewart and D. E. Spearot, Atomistic simulations of nanoindentation on the basal plane of crystalline molyb-

denum disulfide (MoS_2), *Model. Simul. Mater. Sci. Eng.* 21(4), 045003 (2013)

40. J. D. Gale, Gulp: A computer program for the symmetry-adapted simulation of solids, *J. Chem. Soc., Faraday Trans.* 93(4), 629 (1997) (Code available from https://projects.ivec.org/gulp/.)
41. Lammps, http://www.cs.sandia.gov/~sjplimp/lammps.html (2012)
42. S. Jiménez Sandoval, D. Yang, R. F. Frindt, and J. C. Irwin, Raman study and lattice dynamics of single molecular layers of MoS_2, *Phys. Rev. B* 44(8), 3955 (1991)
43. E. Dobardžić, I. Milosevic, B. Dakic, and M. Damnjanovic, Raman and infrared-active modes in MS_2 nanotubes (M=Mo,W), *Phys. Rev. B* 74(3), 033403 (2006)
44. M. Damnjanovic, E. Dobardzic, I. Miloeevic, M. Virsek, and M. Remskar, Phonons in MoS_2 and WS_2 nanotubes, *Mater. Manuf. Process.* 23(6), 579 (2008)
45. H. Wang, Y. Wang, X. Cao, M. Feng, and G. Lan, Vibrational properties of graphene and graphene layers, *Journal of Raman Spectroscopy* 40(12), 1791 (2009)
46. X. Zhang, W. Han, J. Wu, S. Milana, Y. Lu, Q. Li, A. Ferrari, and P. Tan, Raman spectroscopy of shear and layer breathing modes in multilayer MoS_2, *Phys. Rev. B* 87, 115413 (2013)
47. J. W. Jiang, H. S. Park, and T. Rabczuk, MoS_2 nanoresonators: Intrinsically better than graphene? *Nanoscale* 6(7), 3618 (2014)
48. F. Liu, P. Ming, and J. Li, Ab initio calculation of ideal strength and phonon instability of graphene under tension, *Phys. Rev. B* 76(6), 064120 (2007)
49. F. Hao, D. Fang, and Z. Xu, Mechanical and thermal transport properties of graphene with defects, *Appl. Phys. Lett.* 99(4), 041901 (2011)
50. Z. Ni, H. Bu, M. Zou, H. Yi, K. Bi, and Y. Chen, Anisotropic mechanical properties of graphene sheets from molecular dynamics, *Physica B* 405(5), 1301 (2010)
51. Y. Gao and P. Hao, Mechanical properties of mono-layer graphene under tensile and compressive loading, *Physica E* 41(8), 1561 (2009)
52. Y. Guo, L. Jiang, and W. Guo, Opening carbon nanotubes into zigzag graphene nanoribbons by energy-optimum oxidation, *Phys. Rev. B* 82(11), 115440 (2010)
53. Y. Zheng, N. Wei, Z. Fan, L. Xu, and Z. Huang, Mechanical properties of grafold: A demonstration of strengthened graphene, *Nanotechnology* 22(40), 405701 (2011)
54. Y. Wei, J. Wu, H. Yin, X. Shi, R. Yang, and M. Dresselhaus, The nature of strength enhancement and weakening by pentagonheptagon defects in graphene, *Nat. Mater.* 11(9), 759 (2012)
55. Y. Zhang and C. Pan, Measurements of mechanical properties and number of layers of graphene from nano-indentation, *Diamond Related Materials* 24, 1 (2012)
56. Q. Yue, J. Kang, Z. Shao, X. Zhang, S. Chang, G. Wang, S. Qin, and J. Li, Mechanical and electronic properties of monolayer MoS_2 under elastic strain, *Phys. Lett. A* 376(12–13), 1166 (2012)
57. Y. Huang, J. Wu, and K. C. Hwang, Thickness of graphene and single-wall carbon nanotubes, *Phys. Rev. B* 74(24), 245413 (2006)
58. L. Shen, H. S. Shen, and C. L. Zhang, Temperature-dependent elastic properties of single layer graphene sheets, *Mater. Des.* 31(9), 4445 (2010)
59. T. Han, P. He, Y. Luo, and X. Zhang, Research progress in the mechanical properties of graphene, *Advances in Mechanics* 41(3), 279 (2011)
60. L. Xu, N. Wei, Y. Zheng, Z. Fan, H. Q. Wang, and J. C. Zheng, Graphene-nanotube 3d networks: Intriguing thermal and mechanical properties, *J. Mater. Chem.* 22(4), 1435 (2011)
61. J. W. Jiang, J. S. Wang, and B. Li, Elastic and nonlinear stiffness of graphene: A simple approach, *Phys. Rev. B* 81(7), 073405 (2010)
62. S. Bertolazzi, J. Brivio, and A. Kis, Stretching and breaking of ultrathin MoS_2, *ACS Nano* 5(12), 9703 (2011)
63. R. C. Cooper, C. Lee, C. A. Marianetti, X. Wei, J. Hone, and J. W. Kysar, Erratum: Nonlinear elastic behavior of two-dimensional molybdenum disulfide [*Phys. Rev. B* 87, 035423 (2013)], *Phys. Rev. B* 87(7), 079901 (2013)
64. K. Liu, Q. Yan, M. Chen, W. Fan, Y. Sun, J. Suh, D. Y. Fu, S. Lee, J. Zhou, S. Tongay, J. Ji, J. B. Neaton, and J. Q. Wu, Elastic properties of chemical-vapor-deposited monolayer MoS_2, WS_2, and their bilayer heterostructures, arXiv: 1407.2669 (2014)
65. A. Castellanos-Gomez, M. Poot, G. A. Steele, H. S. J. van der Zant, N. Agrait, and G. Rubio-Bollinger, Elastic properties of freely suspended MoS_2 nano sheets, *Adv. Mater.* 24(6), 772 (2012)
66. E. Cadelano, P. L. Palla, S. Giordano, and L. Colombo, Nonlinear elasticity of monolayer graphene, *Phys. Rev. Lett.* 102(23), 235502 (2009)
67. C. D. Reddy, S. Rajendran, and K. M. Liew, Equilibrium configuration and continuum elastic properties of finite sized graphene, *Nanotechnology* 17(3), 864 (2006)
68. H. Zhao, K. Min, and N. R. Aluru, Size and chirality dependent elastic properties of graphene nanoribbons under uniaxial tension, *Nano Lett.* 9(8), 3012 (2009)
69. P. Tao, H. Guo, T. Yang, and Z. Zhang, Strain-induced magnetism in MoS_2 monolayer with defects, *J. Appl. Phys.* 115(5), 054305 (2014)
70. Y. C. Lin, D. O. Dumcenco, Y. S. Huang, and K. Suenaga, Atomic mechanism of the semiconducting-to-metallic phase transition in single-layered MoS_2, *Nat. Nanotechnol.* 9(5), 391 (2014)
71. J. W. Jiang, Phonon bandgap engineering of strained monolayer MoS_2, *Nanoscale* 6(14), 8326 (2014)

72. M. Kan, J. Y. Wang, X. W. Li, S. H. Zhang, Y. W. Li, Y. Kawazoe, Q. Sun, and P. Jena, Structures and phase transition of a MoS_2 monolayer, *J. Phys. Chem. C* 118(3), 1515 (2014)

73. K. Q. Dang, J. P. Simpson, and D. E. Spearot, Phase transformation in monolayer molybdenum disulphide (MoS_2) under tension predicted by molecular dynamics simulations, *Scr. Mater.* 76, 41 (2014)

74. Y. Wei, B. Wang, J. Wu, R. Yang, and M. L. Dunn, Bending rigidity and gaussian bending stiffness of single-layered graphene, *Nano Lett.* 13(1), 26 (2013)

75. X. Zhou, J. J. Zhou, and Z. C. Ou-Yang, Strain energy and Young's modulus of single-wall carbon nanotubes calculated from electronic energy-band theory, *Phys. Rev. B* 62(20), 13692 (2000)

76. T. Ma, B. Li, and T. Chang, Chirality- and curvature-dependent bending stiffness of single layer graphene, *Appl. Phys. Lett.* 99(20), 201901 (2011)

77. Y. Shen and H. Wu, Interlayer shear effect on multilayer graphene subjected to bending, *Appl. Phys. Lett.* 100(10), 101909 (2012)

78. X. Shi, B. Peng, N. M. Pugno, and H. Gao, Stretch-induced softening of bending rigidity in graphene, *Appl. Phys. Lett.* 100(19), 191913 (2012)

79. M. Arroyo and T. Belytschko, Finite crystal elasticity of carbon nanotubes based on the exponential cauchy-born rule, *Phys. Rev. B* 69(11), 115415 (2004)

80. Y. Wang, R. Yang, Z. Shi, L. Zhang, D. Shi, E. Wang, and G. Zhang, Super-elastic graphene ripples for flexible strain sensors, *ACS Nano* 5(5), 3645 (2011)

81. J. Zhang, J. Xiao, X. Meng, C. Monroe, Y. Huang, and J. M. Zuo, Free folding of suspended graphene sheets by random mechanical stimulation, *Phys. Rev. Lett.* 104(16), 166805 (2010)

82. J. X. Shi, Q. Q. Ni, X. W. Lei, and T. Natsuki, Nonlocal elasticity theory for the buckling of double-layer graphene nanoribbons based on a continuum model, *Comput. Mater. Sci.* 50(11), 3085 (2011)

83. C. Wang, L. Lan, and H. Tan, The physics of wrinkling in graphene membranes under local tension, *Phys. Chem. Chem. Phys.* 15(8), 2764 (2013)

84. S. Timoshenko and S. Woinowsky-Krieger, Theory of Plates and Shells, 2nd Ed., New York: McGraw-Hill, 1987

85. J. W. Jiang, The buckling of single-layer MoS_2 under uniaxial compression, *Nanotechnology* 25(35), 355402 (2014)

86. M. Zhou, Y. Zhai, and S. Dong, Electrochemical sensing and biosensing platform based on chemically reduced graphene oxide, *Anal. Chem.* 81(14), 5603 (2009)

87. Y. Xu, C. Chen, V. V. Deshpande, F. A. DiRenno, A. Gondarenko, D. B. Heinz, S. Liu, P. Kim, and J. Hone, Radio frequency electrical transduction of graphene mechanical resonators, *Appl. Phys. Lett.* 97(24), 243111 (2010)

88. X. Q. He, S. Kitipornchai, and K. M. Liew, Resonance analysis of multi-layered graphene sheets used as nanoscale resonators, *Nanotechnology* 16(10), 2086 (2005)

89. Y. Liu, Z. Xu, and Q. Zheng, The interlayer shear effect on graphene multilayer resonators, *J. Mech. Phys. Solids* 59(8), 1613 (2011)

90. J. Wang, X. He, S. Kitipornchai, and H. Zhang, Geometrical nonlinear free vibration of multi-layered graphene sheets, *J. Phys. D: Appl. Phys.* 44(13), 135401 (2011)

91. Y. Xu, S. Yan, Z. Jin, and Y. Wang, Quantum-squeezing effects of strained multilayer graphene nems, *Nanoscale Res. Lett.* 6(1), 355 (2011)

92. F. Gu, J. H. Zhang, L. J. Yang, and B. Gu, Molecular dynamics simulation of resonance properties of strain graphene nanoribbons, *Acta Phys. Sin.* 60(5), 056103 (2011)

93. Z. B. Shen, H. L. Tang, D. K. Li, and G. J. Tang, Vibration of single-layered graphene sheet-based nanomechanical sensor via nonlocal Kirchhoff plate theory, *Comput. Mater. Sci.* 61, 200 (2012)

94. S. M. Zhou, L. P. Sheng, and Z. B. Shen, Transverse vibration of circular graphene sheet-based mass sensor via nonlocal Kirchhoff plate theory, *Comput. Mater. Sci.* 86, 73 (2014)

95. K. L. Ekinci and M. L. Roukes, Nanoelectromechanical systems, *Rev. Sci. Instrum.* 76(6), 061101 (2005)

96. A. M. Zande, R. A. Barton, J. S. Alden, C. S. Ruiz-Vargas, W. S. Whitney, P. H. Q. Pham, J. Park, J. M. Parpia, H. G. Craighead, and P. L. McEuen, Large-scale arrays of single-layer graphene resonators, *Nano Lett.* 10(12), 4869 (2010)

97. C. Chen, S. Rosenblatt, K. I. Bolotin, W. Kalb, P. Kim, I. Kymissis, H. L. Stormer, T. F. Heinz, and J. Hone, Performance of monolayer graphene nanomechanical resonators with electrical read-out, *Nat. Nanotechnol.* 4(12), 861 (2009)

98. J. W. Jiang, B. S. Wang, H. S. Park, and T. Rabczuk, Adsorbate migration effects on continuous and discontinuous temperature-dependent transitions in the quality factors of graphene nanoresonators, *Nanotechnology* 25(2), 025501 (2014)

99. C. Edblom and A. Isacsson, Diffusion-induced dissipation and mode coupling in nanomechanical resonators, arXiv: 1406.1365v1 (2014)

100. A. Eichler, J. Moser, J. Chaste, M. Zdrojek, I. Wilson-Rae, and A. Bachtold, Nonlinear damping in mechanical resonators made from carbon nanotubes and graphene, *Nat. Nanotechnol.* 6(6), 339 (2011)

101. A. Castellanos-Gomez, R. van Leeuwen, M. Buscema, H. S. J. van der Zant, G. A. Steele, and W. J. Venstra, Single-layer MoS_2 mechanical resonators, *Adv. Mater.* 25(46), 6719 (2013)

102. J. Lee, Z. Wang, K. He, J. Shan, and P. X. L. Feng, High frequency MoS_2 nanomechanical resonators, *ACS Nano* 7(7), 6086 (2013)

103. A. A. Balandin, Low-frequency 1/f noise in graphene devices, *Nat. Nanotechnol.* 8(8), 549 (2013)

104. Y. M. Lin and P. Avouris, Strong suppression of electrical noise in bilayer graphene nanodevices, *Nano Lett.* 8(8), 2119 (2008)

105. A. N. Pal and A. Ghosh, Resistance noise in electrically biased bilayer graphene, *Phys. Rev. Lett.* 102(12), 126805 (2009)

106. Z. Cheng, Q. Li, Z. Li, Q. Zhou, and Y. Fang, Suspended graphene sensors with improved signal and reduced noise, *Nano Lett.* 10(5), 1864 (2010)

107. S. Rumyantsev, G. Liu, W. Stillman, M. Shur, and A. A. Balandin, Electrical and noise characteristics of graphene field-effect transistors: Ambient effects, noise sources and physical mechanisms, *J. Phys.: Condens. Matter* 22(39), 395302 (2010)

108. G. Liu, S. Rumyantsev, M. Shur, and A. A. Balandin, Graphene thickness-graded transistors with reduced electronic noise, *Appl. Phys. Lett.* 100(3), 033103 (2012)

109. M. Z. Hossain, S. L. Roumiantsev, M. Shur, and A. A. Balandin, Reduction of 1/f noise in graphene after electron-beam irradiation, *Appl. Phys. Lett.* 102(15), 153512 (2013)

110. K. Saito, J. Nakamura, and A. Natori, Ballistic thermal conductance of a graphene sheet, *Phys. Rev. B* 76(11), 115409 (2007)

111. S. Yien, V. Tayari, J. O. Island, J. M. Porter, and A. R. Champagne, Electronic thermal conductivity measurements in intrinsic graphene, *Phys. Rev. B* 87(24), 241411 (2013)

112. J. S. Wang, J. Wang, and J. T. Lü, Quantum thermal transport in nanostructures, *Eur. Phys. J. B* 62(4), 381 (2008)

113. J. S. Wang, B. K. Agarwalla, H. Li, and J. Thingna, Nonequilibrium greens function method for quantum thermal transport, *Front. Phys.* 9(6), 673 (2013)

114. S. Chen, Q. Wu, C. Mishra, J. Kang, H. Zhang, K. Cho, W. Cai, A. A. Balandin, and R. S. Ruoff, Thermal conductivity of isotopically modified graphene, *Nat. Mater.* 11(3), 203 (2012)

115. Z. Guo, D. Zhang, and X. G. Gong, Thermal conductivity of graphene nanoribbons, *Appl. Phys. Lett.* 95(16), 163103 (2009)

116. Y. Xu, X. Chen, B. L. Gu, and W. Duan, Intrinsic anisotropy of thermal conductance in graphene nanoribbons, *Appl. Phys. Lett.* 95(23), 233116 (2009)

117. S. Chen, A. L. Moore, W. Cai, J. W. Suk, J. An, C. Mishra, C. Amos, C. W. Magnuson, J. Kang, L. Shi, and R. S. Ruoff, Raman measurements of thermal transport in suspended monolayer graphene of variable sizes in vacuum and gaseous environments, *ACS Nano* 5(1), 321 (2011)

118. N. Wei, L. Xu, H. Q. Wang, and J. C. Zheng, Strain engineering of thermal conductivity in graphene sheets and nanoribbons: A demonstration of magic flexibility, *Nanotechnology* 22(10), 105705 (2011)

119. Z. Wei, Z. Ni, K. Bi, M. Chen, and Y. Chen, In-plane lattice thermal conductivities of multilayer graphene films, *Carbon* 49(8), 2653 (2011)

120. Z. X. Xie, K. Q. Chen, and W. Duan, Thermal transport by phonons in zigzag graphene nanoribbons with structural defects, *J. Phys.: Condens. Matter* 23(31), 315302 (2011)

121. X. Zhai and G. Jin, Stretching-enhanced ballistic thermal conductance in graphene nanoribbons, *Europhys. Lett.* 96(1), 16002 (2011)

122. X. F. Peng, X. J. Wang, Z. Q. Gong, and K. Q. Chen, Ballistic thermal conductance in graphene nanoribbon with double-cavity structure, *Appl. Phys. Lett.* 99(23), 233105 (2011)

123. F. Ma, H. B. Zheng, Y. J. Sun, D. Yang, K. W. Xu, and P. K. Chu, Strain effect on lattice vibration, heat capacity, and thermal conductivity of graphene, *Appl. Phys. Lett.* 101(11), 111904 (2012)

124. Z. X. Guo, J. W. Ding, and X. G. Gong, Substrate effects on the thermal conductivity of epitaxial graphene nanoribbons, *Phys. Rev. B* 85(23), 235429 (2012)

125. N. Mingo and D. A. Broido, Carbon nanotube ballistic thermal conductance and its limits, *Phys. Rev. Lett.* 95(9), 096105 (2005)

126. N. Mingo and D. A. Broido, Length dependence of carbon nanotube thermal conductivity and the "problem of long waves", *Nano Lett.* 5(7), 1221 (2005)

127. D. L. Nika, E. P. Pokatilov, A. S. Askerov, and A. A. Balandin, Phonon thermal conduction in graphene: Role of umklapp and edge roughness scattering, *Phys. Rev. B* 79(15), 155413 (2009)

128. D. L. Nika, A. S. Askerov, and A. A. Balandin, Anomalous size dependence of the thermal conductivity of graphene ribbons, *Nano Lett.* 12(6), 3238 (2012)

129. X. Xu, L. F. Pereira, Y. Wang, J. Wu, K. Zhang, X. Zhao, S. Bae, C. Tinh Bui, R. Xie, J. T. L. Thong, B. H. Hong, K. P. Loh, D. Donadio, B. Li, and B. Özyilmaz, Length-dependent thermal conductivity in suspended single-layer graphene, *Nat. Commun.* 5, 3689 (2014)

130. D. L. Nika, E. P. Pokatilov, and A. A. Balandin, Theoretical description of thermal transport in graphene: The issues of phonon cut-off frequencies and polarization branches, *Phys. Status Solidi B* 248(11), 2609 (2011)

131. J. Wang, X. M. Wang, Y. F. Chen, and J. S. Wang, Dimensional crossover of thermal conductance in graphene nanoribbons: A first-principles approach, *J. Phys.: Condens. Matter* 24(29), 295403 (2012)

132. D. L. Nika and A. A. Balandin, Two-dimensional phonon transport in graphene, *J. Phys.: Condens. Matter* 24(23), 233203 (2012)

133. N. Li, J. Ren, L. Wang, G. Zhang, P. Hänggi, and B. Li, Phononics: Manipulating heat flow with electronic analogs and beyond, *Rev. Mod. Phys.* 84(3), 1045 (2012)

134. J. W. Jiang, J. Lan, J. S. Wang, and B. Li, Iso-topic effects on the thermal conductivity of graphene nanoribbons: Localization mechanism, *J. Appl. Phys.* 107(5), 054314 (2010)

135. W. Cai, A. L. Moore, Y. Zhu, X. Li, S. Chen, L. Shi, and R. S. Ruoff, Thermal transport in suspended and supported monolayer graphene grown by chemical vapor deposition, *Nano Lett.* 10(5), 1645 (2010)

136. A. A. Balandin, S. Ghosh, W. Bao, I. Calizo, D. Teweldebrhan, F. Miao, and C. N. Lau, Superior thermal conductivity of single-layer graphene, *Nano Lett.* 8(3), 902 (2008)

137. S. Ghosh, I. Calizo, D. Teweldebrhan, E. P. Pokatilov, D. L. Nika, A. A. Balandin, W. Bao, F. Miao, and C. N. Lau, Extremely high thermal conductivity of graphene: Prospects for thermal management applications in nanoelectronic circuits, *Appl. Phys. Lett.* 92(15), 151911 (2008)

138. L. Lindsay, D. A. Broido, and N. Mingo, Flexural phonons and thermal transport in multilayer graphene and graphite, *Phys. Rev. B* 83(23), 235428 (2011)

139. Z. Aksamija and I. Knezevic, Lattice thermal conductivity of graphene nanoribbons: Anisotropy and edge roughness scattering, *Appl. Phys. Lett.* 98(14), 141919 (2011)

140. L. Chen and S. Kumar, Thermal transport in graphene supported on copper, *J. Appl. Phys.* 112(4), 043502 (2012)

141. Z. Wei, J. Yang, K. Bi, and Y. Chen, Mode dependent lattice thermal conductivity of single layer graphene, *J. Appl. Phys.* 116(15), 153503 (2014)

142. S. Ghosh, W. Bao, D. L. Nika, S. Subrina, E. P. Pokatilov, C. N. Lau, and A. A. Balandin, Dimensional crossover of thermal transport in few-layer graphene, *Nat. Mater.* 9(7), 555 (2010)

143. D. Singh, J. Y. Murthy, and T. S. Fisher, Mechanism of thermal conductivity reduction in few-layer graphene, *J. Appl. Phys.* 110(4), 044317 (2011)

144. G. Zhang and H. Zhang, Thermal conduction and rectification in few-layer graphene y junctions, *Nanoscale* 3(11), 4604 (2011)

145. W.R. Zhong, M.P. Zhang, B.Q. Ai, and D.Q. Zheng, Chirality and thickness-dependent thermal conductivity of few-layer graphene: A molecular dynamics study, *Appl. Phys. Lett.* 98(11), 113107 (2011)

146. W. R. Zhong, W. H. Huang, X. R. Deng, and B. Q. Ai, Thermal rectification in thickness-asymmetric graphene nanoribbons, *Appl. Phys. Lett.* 99(19), 193104 (2011)

147. A. Rajabpour and S. M. Vaez Allaei, Tuning thermal conductivity of bilayer graphene by inter-layer sp3 bonding: A molecular dynamics study, *Appl. Phys. Lett.* 101(5), 053115 (2012)

148. H. Y. Cao, Z. X. Guo, H. Xiang, and X. G. Gong, Layer and size dependence of thermal conductivity in multilayer graphene nanoribbons, *Phys. Lett. A* 376(4), 525 (2012)

149. T. Sun, J. Wang, and W. Kang, Van der waals interaction-tuned heat transfer in nanostructures, *Nanoscale* 5(1), 128 (2012)

150. S. Sahoo, A. P. S. Gaur, M. Ahmadi, M. J. F. Guinel, and R. S. Katiyar, Temperature dependent raman studies and thermal conductivity of few layer MoS_2, *J. Phys. Chem. C* 117(17), 9042 (2013)

151. V. Varshney, S. S. Patnaik, C. Muratore, A. K. Roy, A. A. Voevodin, and B. L. Farmer, Md simulations of molybdenum disulphide (MoS_2): Force-field parameterization and thermal transport behavior, *Comput. Mater. Sci.* 48(1), 101 (2010)

152. W. Huang, H. Da, and G. Liang, Thermoelectric performance of MX_2 (M=Mo, W; X=S, Se) monolayers, *J. Appl. Phys.* 113(10), 104304 (2013)

153. J. W. Jiang, X. Y. Zhuang, and T. Rabczuk, Orientation dependent thermal conductance in single-layer MoS_2, *Scientific Reports* 3, 2209 (2013)

154. J. W. Jiang, J. S. Wang, and B. Li, Thermal conductance of graphene and dimerite, *Phys. Rev. B* 79(20), 205418 (2009)

155. X. Liu, G. Zhang, Q. X. Pei, and Y. W. Zhang, Phonon thermal conductivity of monolayer MoS_2 sheet and nanoribbons, *Appl. Phys. Lett.* 103(13), 133113 (2013)

156. Z. Yan, G. Liu, J. M. Khan, and A. A. Balandin, Graphene quilts for thermal management of high-power gan transistors, *Nat. Commun.* 3, 827 (2012)

157. V. Goyal and A. A. Balandin, Thermal properties of the hybrid graphene-metal nano-micro-composites: Applications in thermal interface materials, *Appl. Phys. Lett.* 100(7), 073113 (2012)

158. K. M. F. Shahil and A. A. Balandin, Graphenemultilayer graphene nanocomposites as highly efficient thermal interface materials, *Nano Lett.* 12(2), 861 (2012)

159. P. Goli, S. Legedza, A. Dhar, R. Salgado, J. Renteria, and A. A. Balandin, Graphene-enhanced hybrid phase change materials for thermal management of Li-ion batteries, *J. Power Sources* 248(15), 37 (2014)

160. H. Malekpour, K. H. Chang, J. C. Chen, C. Y. Lu, D. L. Nika, K. S. Novoselov, and A. A. Balandin, Thermal conductivity of graphene laminate, *Nano Lett.* 14(9), 5155 (2014)

161. P. Song, Z. Cao, Y. Cai, L. Zhao, Z. Fang, and S. Fu, Fabrication of exfoliated graphene-based polypropy-lene nanocomposites with enhanced mechanical and thermal properties, *Polymer* 52(18), 4001 (2011)

162. W. Yu, H. Xie, and D. Bao, Enhanced thermal conductivities of nanofluids containing graphene oxide nanosheets, *Nanotechnology* 21(5), 055705 (2010)

163. W. Yu, H. Xie, and W. Chen, Experimental investigation on thermal conductivity of nanofluids containing graphene oxide nanosheets, *J. Appl. Phys.* 107(9), 094317 (2010)

164. W. Yu, H. Xie, X. Wang, and X. Wang, Significant thermal conductivity enhancement for nanofluids containing graphene nanosheets, *Phys. Lett. A* 375(10), 1323 (2011)

165. Y. Wang, Z. Shi, Y. Huang, Y. Ma, C. Wang, M. Chen, et al., Supercapacitor devices based on graphene materials, *J. Phys. Chem. C* 113, 131030 (2009)

166. K. S. Novoselov, A. K. Geim, S. V. Morozov, D. Jiang, M. I. Katsnelson, I. V. Grigorieva, S. V. Dubonos, and A. A. Firsov, Two-dimensional gas of massless Dirac fermions in graphene, *Nature* 438(7065), 197 (2005)

167. S. Y. Zhou, G. H. Gweon, J. Graf, A. V. Fedorov, C. D. Spataru, R. D. Diehl, Y. Kopelevich, D.H. Lee, S. G. Louie, and A. Lanzara, First direct observation of Dirac fermions in graphite, *Nat. Phys.* 2(9), 595 (2006)

168. B. Partoens and F. M. Peeters, Normal and dirac fermions in graphene multilayers: Tight-binding description of the electronic structure, *Phys. Rev. B* 75(19), 193402 (2007)

169. J. Hass, F. Varchon, J. E. Millan-Otoya, M. Sprinkle, N. Sharma, W. A. de Heer, C. Berger, P. First, L. Magaud, and E. Conrad, Why multi-layer graphene on 4h-sic $000\bar{1}$ behaves like a single sheet of graphene, *Phys. Rev. Lett.* 100(12), 125504 (2008)

170. S. Reich, J. Maultzsch, C. Thomsen, and P. Ordejon, Tight-binding description of graphene, *Phys. Rev. B* 66(3), 035412 (2002)

171. V. Pereira, A. Castro Neto, and N. Peres, Tight-binding approach to uniaxial strain in graphene, *Phys. Rev. B* 80(4), 045401 (2009)

172. F. Guinea, M. I. Katsnelson, and A. K. Geim, Energy gaps and a zero-field quantum hall effect in graphene by strain engineering, *Nat. Phys.* 6(1), 30 (2010)

173. K. Nakada, M. Fujita, G. Dresselhaus, and M. S. Dresselhaus, Edge state in graphene ribbons: Nanometer size effect and edge shape dependence, *Phys. Rev. B* 54(24), 17954 (1996)

174. K. K. Kam and B. A. Parkinson, Detailed photocurrent spectroscopy of the semiconducting group vi transition metal dichalcogenides, *J. Phys. Chem.* 86(4), 463 (1982)

175. T. Eknapakul, P. D. C. King, M. Asakawa, P. Buaphet, R. H. He, S. K. Mo, H. Takagi, K. M. Shen, F. Baumberger, T. Sasagawa, S. Jungthawan, and W. Meevasana, Electronic structure of a quasi-freestanding MoS_2 monolayer, *Nano Lett.* 14(3), 1312 (2014)

176. Y. Li, Z. Zhou, S. Zhang, and Z. Chen, MoS_2 nanorib-bons: High stability and unusual electronic and magnetic properties, *J. Am. Chem. Soc.* 130(49), 16739 (2008)

177. P. Lu, X. Wu, W. Guo, and X. C. Zeng, Strain-dependent electronic and magnetic properties of MoS_2 monolayer, bilayer, nanoribbons and nanotubes, *Phys. Chem. Chem. Phys.* 14(37), 13035 (2012)

178. B. Radisavljevic, A. Radenovic, J. Brivio, V. Giacometti, and A. Kis, Single-layer MoS_2 transistors, *Nat. Nanotechnol.* 6(3), 147 (2011)

179. V. K. Sangwan, H. N. Arnold, D. Jariwala, T. J. Marks, L. J. Lauhon, and M. C. Hersam, Low-frequency electronic noise in single-layer MoS_2 transistors, *Nano Lett.* 13(9), 4351 (2013)

180. E. Scalise, M. Houssa, G. Pourtois, V. Afanasev, and A. Stesmans, Strain-induced semiconductor to metal transition in the two-dimensional honeycomb structure of MoS_2, *Nano Research* 5(1), 43 (2012)

181. H. J. Conley, B. Wang, J. I. Ziegler, R. F. Jr Haglund, S. T. Pantelides, and K. I. Bolotin, Bandgap engineering of strained monolayer and bilayer MoS_2, *Nano Lett.* 13(8), 3626 (2013)

182. K. F. Mak, C. Lee, J. Hone, J. Shan, and T. F. Heinz, Atomically thin MoS_2: A new direct-gap semiconductor, *Phys. Rev. Lett.* 105(13), 136805 (2010)

183. R. R. Nair, P. Blake, A. N. Grigorenko, K. S. Novoselov, T. J. Booth, T. Stauber, N. M. R. Peres, and A. K. Geim, Fine structure constant defines visual transparency of graphene, *Science* 320(5881), 1308 (2008)

184. F. Xia, T. Mueller, Y. Lin, A. Valdes-Garcia, and P. Avouris, Ultrafast graphene photodetector, *Nat. Nanotechnol.* 4(12), 839 (2009)

185. O. Lopez-Sanchez, D. Lembke, M. Kayci, A. Raden-ovic, and A. Kis, Ultrasensitive photodetectors based on monolayer MoS_2, *Nat. Nanotechnol.* 8(7), 497 (2013)

186. C. H. Lui, A. J. Frenzel, D. V. Pilon, Y. H. Lee, X. Ling, G. M. Akselrod, *et al.*, Trion induced negative photoconductivity in monolayer MoS_2, arXiv: 1406.5100 (2014)

187. K. Roy, M. Padmanabhan, S. Goswami, T. P. Sai, S. Kaushal, and A. Ghosh, Optically active heterostructures of graphene and ultrathin MoS_2, *Solid State Commun.* 175–176, 35 (2013)

188. G. Algara-Siller, S. Kurasch, M. Sedighi, O. Lehtinen, and U. Kaiser, The pristine atomic structure of MoS_2 monolayer protected from electron radiation damage by graphene, *Appl. Phys. Lett.* 103(20), 203107 (2013)

189. N. Myoung, K. Seo, S. J. Lee, and G. Ihm, Large current modulation and spin-dependent tunneling of vertical graphene/MoS_2 heterostructures, *ACS Nano* 7(8), 7021 (2013)

190. S. Bertolazzi, D. Krasnozhon, and A. Kis, Nonvolatile memory cells based on MoS_2/graphene heterostructures, *Nano Lett.* 7(4), 3246 (2013)

191. S. Larentis, J. R. Tolsma, B. Fallahazad, D. C. Dillen, K. Kim, A. H. MacDonald, and E. Tutuc, Band offset and negative compressibility in graphene- MoS_2 heterostructures, *Nano Lett.* 14(4), 2039 (2014)

192. W. Zhang, C. P. Chuu, J. K. Huang, C. H. Chen, M. L. Tsai, Y. H. Chang, *et al.*, Ultrahigh-gain photodetectors based on atomically thin graphene-MoS_2 heterostructures, *Scientific Reports* 4, 3826 (2014)

193. F. Xia, X. Hu, Y. Sun, W. Luo, and Y. Huang, Layer-by-layer assembled MoO_2 graphene thin film as a high-capacity and binder-free anode for lithium-ion batteries, *Nanoscale* 4(15), 4707 (2012)

194. W. Zhang, C. P. Chuu, J. K. Huang, C. H. Chen, M. L. Tsai, Y. H. Chang, *et al.*, Ultrahigh-gain photodetectors based on atomically thin graphene-MoS_2 heterostructures, *Scientific Reports* 4, 3826 (2013)

195. H. Xu, D. He, M. Fu, W. Wang, H. Wu, and Y. Wang, Optical identification of MoS_2/graphene heterostructure on SiO_2/Si substrate, *Opt. Express* 22(13), 15969 (2014)

196. L. F. Wang, T. B. Ma, Y. Z. Hu, Q. Zheng, H. Wang, and J. Luo, Superlubricity of two-dimensional fluorographene/MoS_2 heterostructure: A first-principles study, *Nanotechnology* 25(38), 385701 (2014)

197. Y. Ma, Y. Dai, M. Guo, C. Niu, and B. Huang, Graphene adhesion on MoS_2 monolayer: An ab initio study, *Nanoscale* 3(9), 3883 (2011)

198. L. Yu, Y. H. Lee, X. Ling, E. J. G. Santos, Y. C. Shin, Y. Lin, M. Dubey, E. Kaxiras, J. Kong, H. Wang, and T. Palacios, Graphene/MoS_2 hybrid technology for large-scale two-dimensional electronics, *Nano Lett.* 14(6), 3055 (2014)

199. R. H. Miwa and W. L. Scopel, Lithium incorporation at the MoS_2/graphene interface: An ab initio investigation, *J. Phys.: Condens. Matter* 25(44), 445301 (2013)

200. J. W. Jiang and H. S. Park, Mechanical properties of MoS_2/graphene heterostructures, *Appl. Phys. Lett.* 105(3), 033108 (2014)

201. K. K. Karkkainen, A. H. Sihvola, and K. I. Nikoskinen, Effective permittivity of mixtures: Numerical validation by the FDTD method, *IEEE Trans. Geosci. Rem. Sens.* 38(3), 1303 (2000)